Available online at www.sciencedirect.com

ScienceDirect

Procedia Structural Integrity 36 (2022) 386–393

Structural Integrity Procedia

www.elsevier.com/locate/procedia

1st Virtual International Conference "In service Damage of Materials: Diagnostics and Prediction"

# Finite element analysis of reinforced-concrete beam with shape memory alloy under the bending

N. Bykiv*[a], P. Yasniy[a], Yu. Lapusta[b], V. Iasnii[a]

[a]*Ternopil Ivan Puluj National Technical University , Ternopil, Ukraine*
[b]*University Clermont Auvergne, CNRS, SIGMA Clermont, Institute Pascal, Clermont-Ferrand F-63000, France*

**Abstract**

The paper deals with strengthening of the reinforced concrete beam by shape memory alloy at the place of maximum loading and deformation. A structural analysis is performed using FEM to study the behavior of the beam reinforced by steel and shape memory alloys under 3- and 4-point bending. The elasticity of the reinforced concrete beam with NiTi rods slightly increase and depends on loading type. It was revealed, that under the bending in the beam reinforced by shape memory alloy the residual deflection decreases in comparison with traditional reinforcement.



*Keywords:* structural analysis; reinforced concrete beam; shape memory alloys;

## 1. Introduction

Shape memory alloys (SMA), due to their pseudoelastic and good damping properties, are increasingly using in structures. SMA improve the load-bearing capacity of structures or their individual elements under static load by Almeida et al. (2020); Ayoub et al. (2004); Bykiv et al. (2020); Hamid et al. (2018). Due to high damping properties SMA are employed as the main elements in the devices to decrease the dynamic loadings of the structures by Menna et al. (2015) bridges in particular by Fang et al. (2019). Besides, SMA are considered to be the alternative

* Corresponding author. Tel.: +380-98-23-84-310.
*E-mail address:* nazbuk@gmail.com

2452-3216 
10.1016/j.prostr.2022.01.050

strengthening of the structures or their elements being in operation in the seismic regions by Isalgue et al. (2006); Morais et al. (2017); Zafar and Andrawes (2015).

When calculating the elements of structures taking into account the random loading, the cost of materials and construction increases. To protect structures from this type of load, functional materials can be used. During considering SMA as additional reinforcement in concrete beams by Bykiv et al. (2020), there arises the problem of interaction of SMA rods in beams with different types of concrete and various reinforcement methods by Azadpour and Maghsoudi (2020); Gholampour and Ozbakkaloglu (2018). These studies show that the effect of superelasticity is more shown in medium-strength concrete ($f_{ctest}$ = 37.5 MPa), but to the grater extend cause cracks closure in stronger concrete ($f_{ctest}$ = 53.8 MPa). Increasing the percentage of reinforcement in the beams expands the ability to dissipate energy by more than 50%. Therefore, it is important to analyse the behaviour of beams reinforced with shape memory NiTi alloys under loading reported.

## 2. Materials and methods

To model the superelastic properties of SMA rods, the basic thermomechanical properties of $Ni_{55.75}Ti_{44.15}$ alloy were investigated by Bykiv et al. (2021). The temperatures of the phase transformations during heating (Fig.1a) and cooling (Fig.1b) were determined by the method of differential scanning calorimetry. Mechanical properties of SMA (

Table 1) obtained by uniaxial tension of the sample with a diameter of 4 mm are shown on the hysteresis loop (Fig.2).

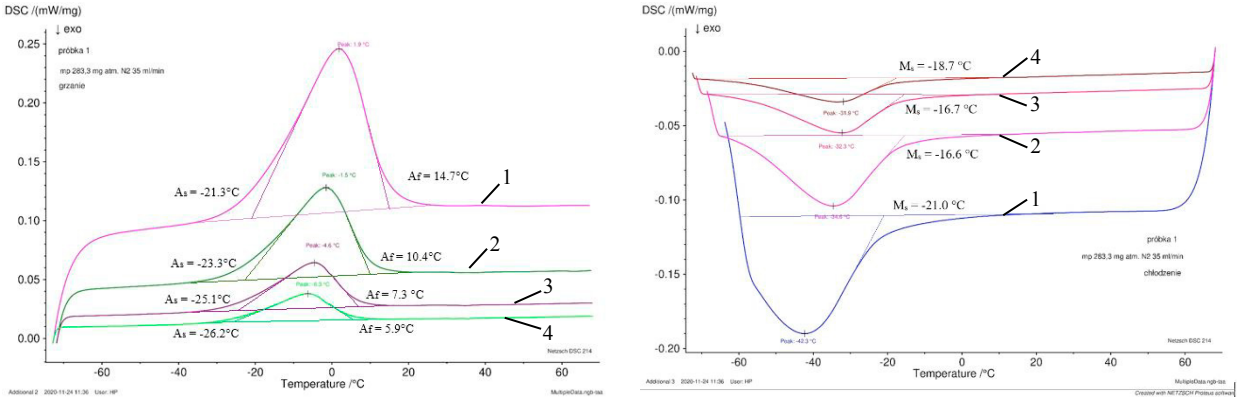


Fig.1. DSC analysis of shape memory alloy at a rate of 10°C/min (1), 5°C/min (2), 2,5°C/min (3) 1,5°C/min (4) heating (a) and cooling (b) mode.

Table 1. Mechanical properties of NiTi used for modelling

| SMA | Density, g/cm$^3$ | Young's module, GPa | Poisson's Ratio | $\sigma_S^{AM}$, MPa | $\sigma_F^{AM}$, MPa | $\sigma_S^{MA}$, MPa | $\sigma_F^{MA}$, MPa | ε, m/m | Alpha |
|---|---|---|---|---|---|---|---|---|---|
| NiTi | 6.45 | 68.2 | 0.36 | 407.5 | 428.3 | 127.2 | 73.6 | 0.06 | 0 |

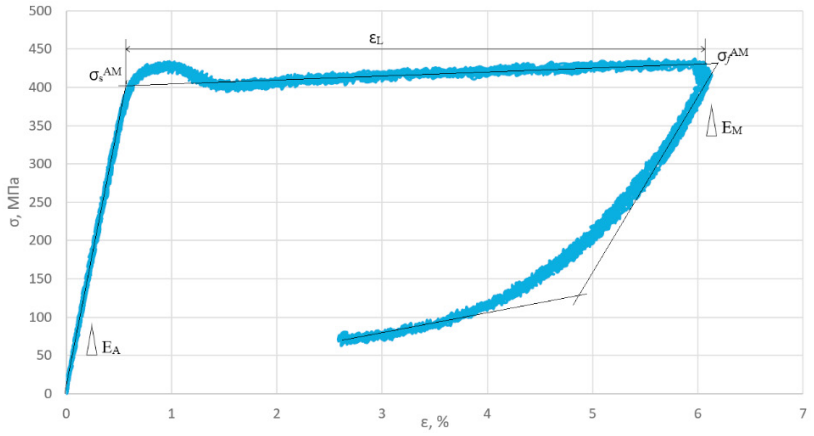


Fig.2. The hysteresis loop of shape memory alloy.

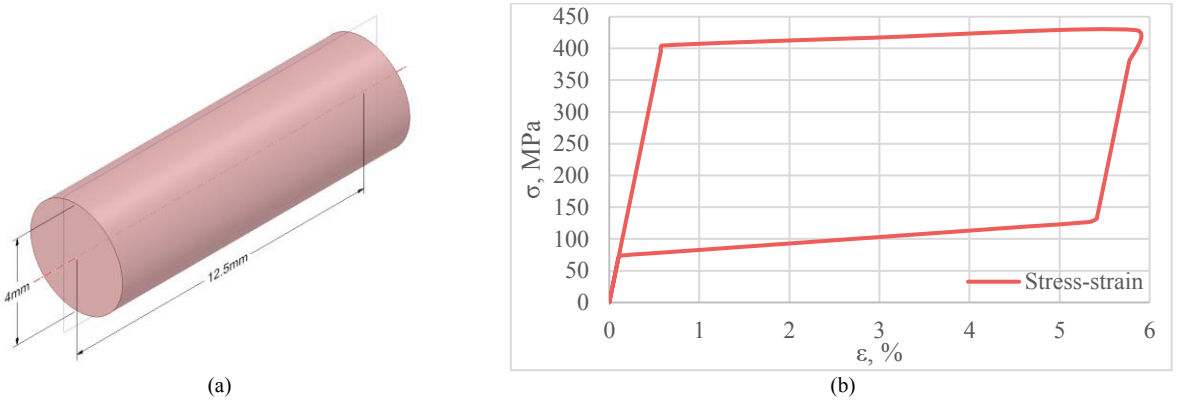


(a) (b)

Fig.3 NiTi sample model (a) and hysteresis loop (b).

To verify the behavior of SMA model, a cylindrical element with a diameter of 4 mm and a length of 12.5 mm was studied (Fig.3a). For this model, the NiTi alloy characteristics obtained from the experiment (

Table 1) were used and loaded with uniaxial tensile with a force of 5.39 kN followed by unloading (Fig.3b). The required force was determined from the following formula:

$$F = \sigma_{FAS} \cdot \pi r^2, \quad (1)$$

where $\sigma_{FAS}$ is the stress of transformation completion; r is the radius of specimen.

The hysteresis loop obtained by modelling corresponds to the experimentally obtained values and the error does not exceed 5%.

A linear structural analysis is performed using FEM to study the behaviour of reinforced concrete beam by steel and SMA under 3- and 4-point bending. The objects of the research were reinforced concrete beam measuring 140x80x1200 mm (Fig.4a), made of concrete C20/25 and 400C 2Ø12 mm working reinforcement (Fig.4b). Inserts of 2Ø8 mm nitinol rods were used at the place of the largest stresses (Fig.4c). The concrete strength data and that of the reinforcement meet the standards of DBN V.2.6-98:2009 and DSTU B V.2.6-156:2010 and are presented in Table 2.

The model of the beam was subjected to bending: in the case of 3-point loading (Fig.5a) the force was applied in the middle of the beam; in the case of 4-point load (Fig.5b) the force was applied at distances of 1/3 of the length of the beam.

Table 2. The main properties of materials

| Material | Density, g/cm³ | Young's module, GPa | Poisson's Ratio | Yield Strength, MPa | Tangent Modulus, MPa | Ultimate Strength, MPa |
|---|---|---|---|---|---|---|
| Concrete | 2.3 | 23 | 0.2 | – | – | 14.5 |
| Steel | 7.85 | 210 | 0.3 | 365 | 4000 | |
| Steel | 7.85 | 210 | 0.3 | 225 | 2500 | |

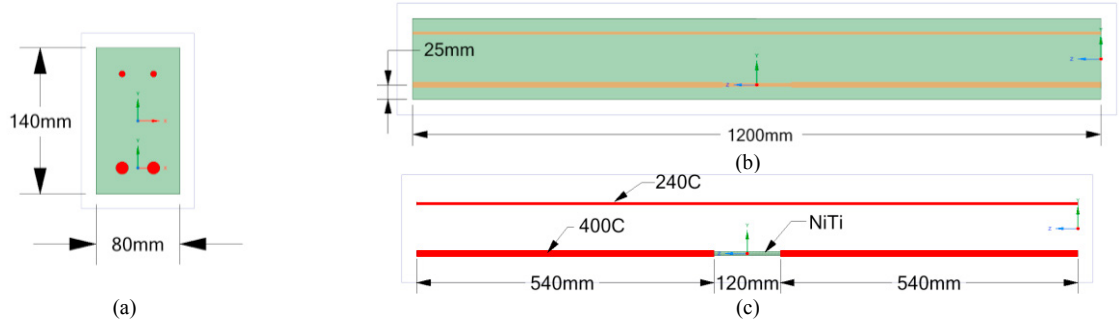


Fig.4. Beam model with SMA rods: (a) cross-section; (b) right side; (c) reinforcement.

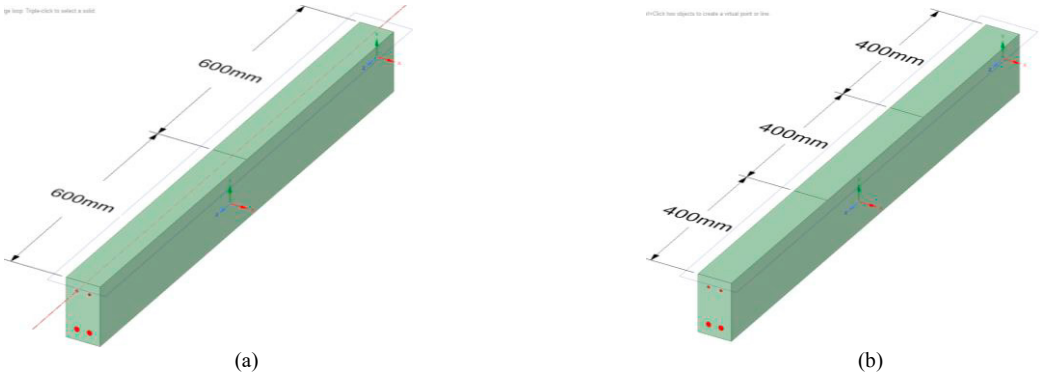


Fig.5. Loading beams: (a) 3-poin; (b) 4-point.

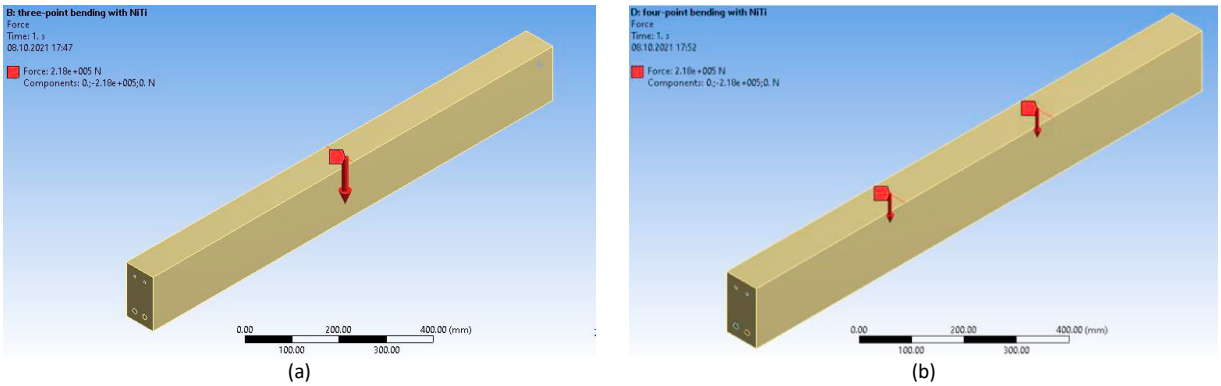


Fig.6. Loading forces of beams: (a) 3-point; (b) 4-point.

The reinforced concrete beam was loaded with a force of 218 kN in both load cases (Fig.6). This force is selected in such a way that the NiTi rods show the effect of superelasticity.

## 3. Results and discussions

As expected, the analysis of the behaviour of the beam with nitinol rods during 3-point and 4-point bending showed that at the same force of 218 kN the beam deflection of 8.6 mm from 3-point loading would be greater than 15.4 mm deflection from 4-point load (Fig. 7). Similarly, the residual deflections can be characterized as well: 1.14 mm and 0.99 mm after 3-point and 4-point loading, respectively.

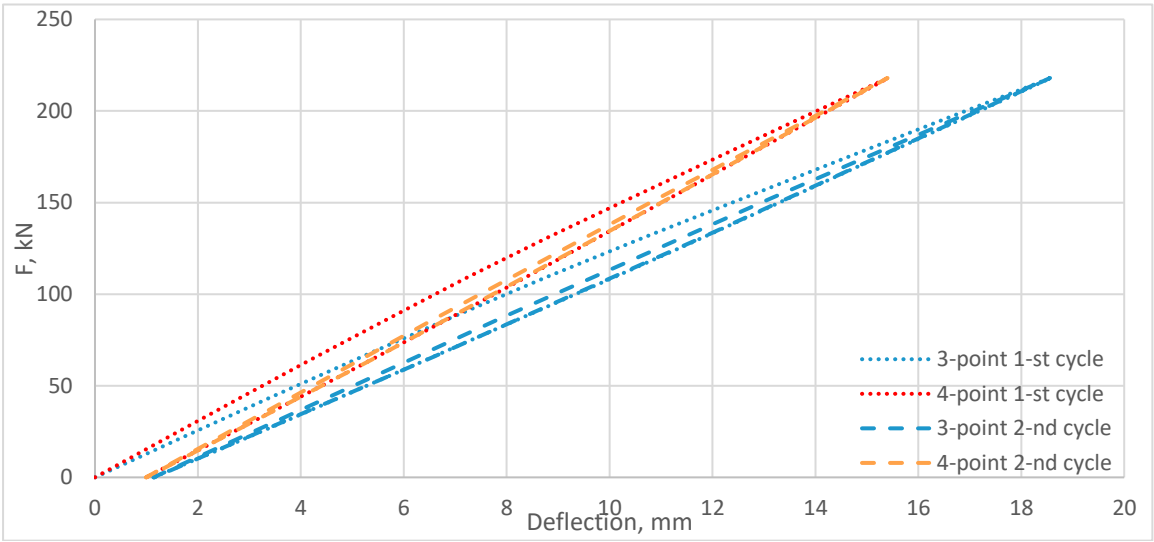


Fig.7. Load-deflection response of reinforced beam by NiTi alloy under 3- and 4-point bending

After beams reloading and unloading the maximum deflections did not change due to the lack of fatigue characteristics in the model for concrete, reinforcement and nitinol in this study. However, the residual deflection increased to 1.16 mm after 3-point loading and to 1 mm after 4-point loading.

The behaviour of reinforcement and nitinol rods in a reinforced concrete beam was analysed in detail on the example of a 3-point loading, where a greater deflection occurred. Thus, at maximum deflection, the maximum stresses in nitinol rods are 408 MPa, while in the reinforcement, the maximum stresses are 382 MPa (Fig.8a). However, it should be noted that the reinforcement was subjected to plastic deformations in areas where stresses exceeded the yield strength $\sigma_{0.2}$ = 365 MPa (Table 2).

After unloading, the residual maximum stresses in the 400C reinforcement are 398 MPa, while the maximum stresses in the nitinol rods are concentrated at the edges and are equal to 113 MPa (Fig. 8b). This can be explained by the fact that on the one hand the stresses in the 400C reinforcement exceeded the yield strength, and on the other hand, the structural steel can restore only 0.2% of maximum elongation, while nitinol can recover up to 6% (Fig.3).

It should be noted that during the second loading cycle, the maximum stresses in the 400C reinforcement increase from 382 MPa to 391 MPa. At the same time, the maximum stresses in the nitinol rods were constant, and the residual stresses decreased from 127 MPa to 113 MPa (Table 3).

Table 3. Maximal and residual stresses of NiTi beam under 3-point bending

| Number of cycle | Type of rebar in beam | Maximal stress, MPa | Residual stress, MPa |
|---|---|---|---|
| First cycle | NiTi | 408 | 127 |

| | | | |
|---|---|---|---|
| Second cycle | 400C | 382 | 388 |
| | NiTi | 408 | 113 |
| | 400C | 391 | 398 |

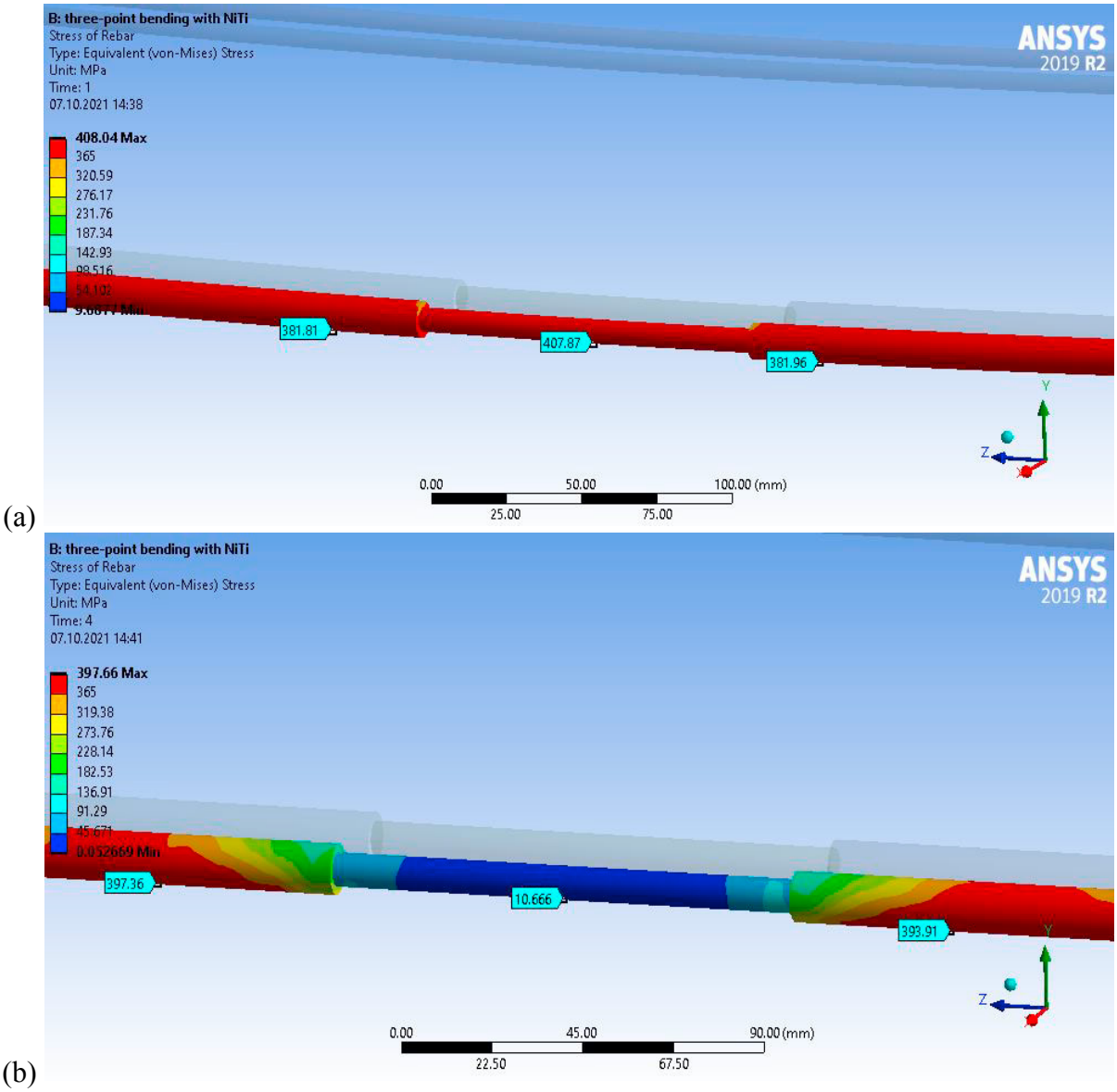


Fig.8. Maximum stress during first cycle (a) and residual stress after second cycle (b) of reinforced element

During the 3-point bending, the beam with SMA rods bent 1.1% more than conventional reinforcement, and during the 4-point bending the deflection in both beams was the same (Fig.9**Помилка! Джерело посилання не знайдено.**). The greater deflection of the beam with SMA rods is due to the fact that the modulus of elasticity of NiTi alloy is smaller than that of 400C reinforcement (Table 2). However, the residual deflections in the beams with

NiTi rods are 24% smaller than in the typical beams in case of 3-point bending, and 27% in case of 4-point bending (Table 4)

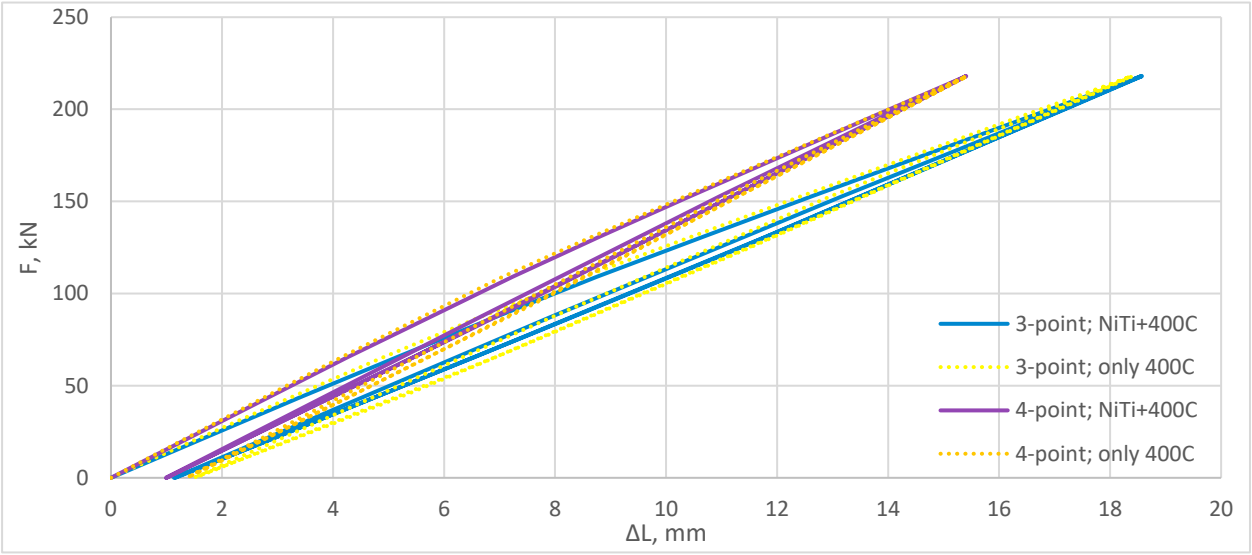


Fig.9. Load-deflection response of reinforced beam by NiTi alloy and only 400C under 3- and 4-point bending

Table 4. Maximal and residual deflections of NiTi beam under 3-point bending

| Bending | Type of reinforcement | Maximum deflection, mm | Residual deflection, mm |
|---|---|---|---|
| 3-point | NiTi+400C | 18.6 | 1.16 |
| | Only 400C | 18.4 | 1.52 |
| 4-point | NiTi+400C | 15.4 | 1 |
| | Only 400C | 15.4 | 1.37 |

It was found that the maximum reinforcement stresses in the beam with nitinol rods exceed the maximum reinforcement stresses in the beam without nitinol rods by 6% in the first cycle and by 0.5% in the second cycle. Nevertheless, the residual reinforcement stresses in the beam with nitinol rods were 2.3% lower in the first cycle and 4.3% lower in the second cycle compared to the reinforcement in the beam without nitinol rods (Table 5).

Table 5. Results of 3-point bending beams

| Number of cycle | Type of reinforcement | Maximum stress, MPa | Residual stress, MPa |
|---|---|---|---|
| First cycle | NiTi+400C | 408 | 388 |
| | Only 400C | 386 | 397 |
| Second cycle | NiTi+400C | 408 | 398 |
| | Only 400C | 406 | 416 |

All in all, the obtained results show that the use of NiTi alloy insertion in structural elements made of structural materials after a load exceeding the allowable, prevents the loss of stability and failure of structures. Due to the effect of superelasticity, residual deformations are much smaller compared to typical materials.

The presented results could be used while designing structures that will be operated under significant deformations.

## 4. Conclusions

The elasticity of the reinforced concrete beam with NiTi rods slightly increase and depends of loading type. However, residual deflection reduces by 24% under 3-point bending and by 27% under 4-point bending in comparison with traditional reinforcement.

In the beam with nitinol rods, the maximum stresses are higher by 6% in the first cycle and 0.5% in the second cycle, but the residual stresses are lower by 2.3% in the first cycle and 4.3% in the second cycle, compared to the beam without nitinol rods.

Residual stresses decreased using NiTi rods by 2.3% after the first cycle; 4.3% after the second cycle. It was estimated that under 4-point bending, NiTi rods showed a better recovery effect in comparison with 3-point bending.

## Rferences

Almeida, J. P. de, Steinmetz, M., Rigot, F., & de Cock, S., 2020. Shape-memory NiTi alloy rebars in flexural-controlled large-scale reinforced concrete walls: Experimental investigation on self-centring and damage limitation. Engineering Structures, 220(April), 110865.

Ayoub, C., Saiid Saiidi, M., & Itani, A., 2004. Study Shape memory alloy Reinforced Beams and Cubes RDT04-046.

Azadpour, F., & Maghsoudi, A. A., 2020. Experimental and analytical investigation of continuous RC beams strengthened by SMA strands under cyclic loading. Construction and Building Materials, 239, 117730.

Bykiv, N., Iasnii, V., Yasniy, P., Junga, R., 2021. Thermomechanical analysis of nitinol memory alloy behavior. Scientific Journal of TNTU (Tern.), 102(2), 161–167.

Bykiv, N., Yasniy, P., Iasnii, V., 2020. Modeling of mechanical behavior of reinforced concrete beam reinforced by the shape memory alloy insertion using finite elements method. Modern Technologies and Methods of Calculations in Construction, 13, 24–34.

Fang, C., Zheng, Y., Chen, J., Yam, M. C. H., & Wang, W., 2019. Superelastic NiTi SMA cables: Thermal-mechanical behavior, hysteretic modelling and seismic application. Engineering Structures, 183, 533–549.

Gholampour, A., & Ozbakkaloglu, T., 2018. Understanding the compressive behavior of shape memory alloy (SMA)-confined normal- and high-strength concrete. Composite Structures, 202, 943–953.

Hamid, N. A., Ibrahim, A., Adnan, A., & Ismail, M. H., 2018. Behaviour of smart reinforced concrete beam with super elastic shape memory alloy subjected to monotonic loading. AIP Conference Proceedings, 1958.

Isalgue, A., Lovey, F. C., Terriault, P., Martorell, Torra, F. R. M., & Torra, V., 2006. SMA for Dampers in Civil Engineering. Materials Transactions, 47(3), 682–690.

Menna, C., Auricchio, F., & Asprone, D., 2015. Applications of shape memory alloys in structural engineering. In Shape Memory Alloy Engineering.

Morais, J., de Morais, P. G., Santos, C., Costa, A. C., & Candeias, P., 2017. Shape Memory Alloy Based Dampers for Earthquake Response Mitigation. Procedia Structural Integrity, 5, 705–712.

Zafar, A., & Andrawes, B., 2015. Seismic behavior of SMA–FRP reinforced concrete frames under sequential seismic hazard. Engineering Structures, 98, 163–173.